JOURNAL OF SOLID STATE CHEMISTRY **122,** 297–302 (1996)
ARTICLE NO. 0116

Spin State of Cobalt Ion in $Nd(Cr_{1-x}Co_x)O_3$

Hideki Taguchi

Research Laboratory for Surface Science, Faculty of Science, Okayama University, Okayama 700, Japan

Received September 14, 1995; in revised form December 5, 1995; accepted December 12, 1995

Perovskite-type $Nd(Cr_{1-x}CO_x)O_3$ was synthesized in the range $0 \leq x \leq 1.0$, and has the orthorhombic $GdFeO_3$-type structure with space group *Pnma*. The decrease of the average (Cr, Co)–O distance and the effective magnetic moment (μ_{eff}) indicate that the Co^{3+} ion in $Nd(Cr_{1-x}CO_x)O_3$ is in the low-spin state $(d\varepsilon)^6(d\gamma)^0$ at low temperature. With increasing temperature, the $1/\chi$-T curve exhibits the plateau, and this plateau indicates the temperature interval where there is a conversion from the low-spin state of the Co^{3+} ion to a mixed spin state. From the results of the electrical resistivity (ρ), $Nd(Cr_{1-x}Co_x)O_3$ is semiconductive with the energy gap (E_g) of ≈0.36–0.47 eV. The log ρ-1000/T curves at high temperature deviate from those at low temperature. Rietveld analysis indicates that each (Cr, Co)O_6 octahedron has little distortion and that the average angles for (Cr, Co)–O(1 and 2)–(Cr, Co) increase with increasing x, in agreement with the decrease in the average (Cr, Co)–O distance. Therefore, it is apparent that the magnetic and electrical properties of $Nd(Cr_{1-x}Co_x)O_3$ depend on the spin state of the Co^{3+} ion and a cation–anion–cation overlap.

INTRODUCTION

Raccah and Goodenough (1) reported the coexistence of the low-spin and high-spin states of cobalt in $LaCoO_3$ and a first-order phase change at 1210 K. The first-order phase change is a localized-electron ↔ collective-electron phase change for electrons in orbitals of e_g symmetry. Below 398 K, $LaCoO_3$ is a semiconductor with a conductivity (σ) given by $\sigma = \sigma_0 \exp(-E/kT)$. The conductivity increases much more rapidly with increasing temperature in the interval $398 < T < 923$ K. In the interval $923 < T < 1210$ K, the conductivity goes through a broad peak and has a maximum value. Above 1210 K, the conductivity decreases with increasing temperature.

Recently, Senaris-Rodriguez and Goodenough (2) prepared homogeneous $LaCoO_3$ from coprecipitated precursors, and investigated the spin state of cobalt ions. A first-order phase change near 1200 K only appears when Co_3O_4 is present as an impurity phase. In the interval $110 < T < 350$ K, a mixture of approximately 50% high-spin and 50% low-spin cobalt forms an ordered semiconductive phase. The metallic high-temperature phase for $T > 650$ K is nucleated and grows with increasing temperature in the interval $350 < T < 620$ K.

Madhusudan *et al.* (3) reported that rare-earth trioxocobaltates, $LnCoO_3$ (Ln = Pr, Nd, Tb, Dy, and Yb), exhibit low-spin to high-spin transitions of cobalt. The susceptibility behavior of solid solutions of $(La_{1-x}Nd_x)CoO_3$ has been investigated to see how the behavior characteristic of $NdCoO_3$ changes to that of $LaCoO_3$. $NdCoO_3$ is pseudo-tetragonal with orthorhombic symmetry and the $GdFeO_3$-type structure with a = 0.5345 nm, b = 0.7560 nm, and c = 0.5345 nm (4). From the magnetic measurement, the spin state of cobalt changes at ≈240 K.

$NdCrO_3$ also has the orthorhombic $GdFeO_3$-type structure with a = 0.5430 nm, b = 0.7692 nm, and c = 0.5488 nm, and exhibits antiferromagnetism with a Néel temperature (T_N) of 224 K (5, 6). The magnetic susceptibility indicates that the electron configuration of Cr^{3+} ions is $(d\varepsilon)^3$ $(d\gamma)^0$. From the temperature dependence of the electrical resistivity (ρ), $NdCrO_3$ exhibits a p-type semiconducting behavior above room temperature (5). The activation energy (E_a) calculated from the linear portion of the log ρ-1000/T curve is ≈0.28 eV (7).

Taguchi (8) investigated the relationship between the electrical properties and a cation–anion–cation overlap in $Nd(Cr_{1-x}Mn_x)O_3$. The average (Cr, Mn)–O distance and the effective magnetic moment (μ_{eff}) indicate that the spin state of the Mn^{3+} ion is high. $Nd(Cr_{1-x}Mn_x)O_3$ is a semiconductor and has a maximum activation energy (E_a) at x = 0.2. The overlap between the cation $d\varepsilon$ and oxygen p_π orbitals plays an important role in the electrical properties of $Nd(Cr_{1-x}Mn_x)O_3$. The ionic radius of the Co^{3+} ion is smaller than the ionic radius of the Mn^{3+} ion (9). Therefore, it is apparent that the (Cr, Co)–O distance in $Nd(Cr_{1-x}Co_x)O_3$ decreases with increasing x. It is very interesting to investigate the relationship between the cation–anion–cation overlap in $Nd(Cr_{1-x}Co_x)O_3$ and the physical properties.

In the present study, $Nd(Cr_{1-x}Co_x)O_3$ was synthesized to study its electrical properties, magnetic properties, and

0022-4596/96 $18.00

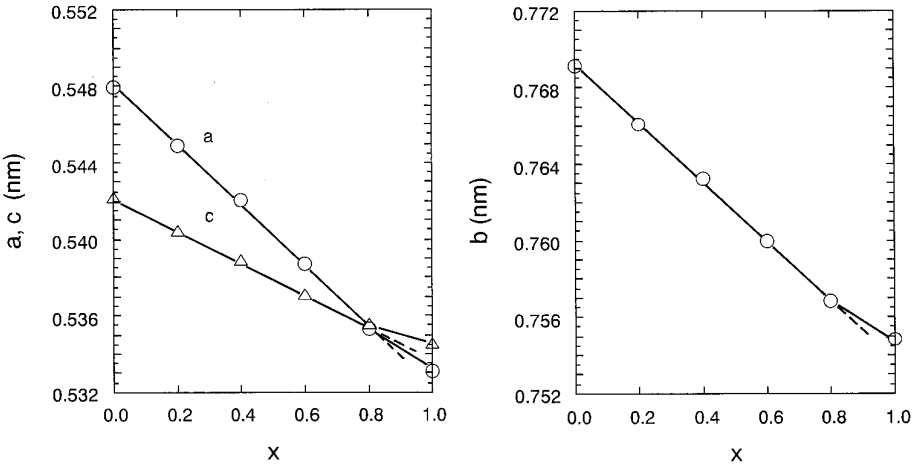

FIG. 1. Cell constants vs composition for the system $Nd(Cr_{1-x}Co_x)O_3$.

the structure refinement. These results will provide information regarding the cation–anion–cation overlap in $Nd(Cr_{1-x}Co_x)O_3$.

EXPERIMENTAL

$Nd(Cr_{1-x}Co_x)O_3$ was prepared by a standard ceramic technique. Dried Nd_2O_3, Cr_2O_3, and $2CoCO_3 \cdot 3Co(OH)_2$ powders were weighed in the appropriate proportions and milled for a few hours with acetone. After the mixed powders were dried at 373 K, they were calcined at 1173 K for a few hours in air, and then fired 1573 K for 24 h in a flow of pure oxygen gas. In order to measure the electrical resistivities, the powders were pressed into a pellet form under a pressure of 50 MPa, and the pellet was sintered at 1573 K for 12 h in the flow of pure oxygen gas.

The phases of the samples were identified by X-ray powder diffraction (XRD) with monochromatic Cu$K\alpha$ radiation. The cell constants of the samples were determined from high-angle reflections with Si as an external standard. The structure refinement was carried out by Rietveld analysis of the XRD data with the RIETAN program written by Izumi (10). XRD data were collected by step scanning over the angular range $20° \leq 2\theta \leq 100°$ in increments of $0.02°$ (2θ) with monochromatic Cu$K\alpha$ radiation.

The electrical resistivity of the samples was measured by a standard four-electrode technique in the interval $150 \leq T \leq 1253$ K. The magnetic susceptibility was measured by a magnetic torsion balance in the interval $80 \leq T \leq 763$ K. Differential thermal analysis (DTA) of the sample was performed in the interval $300 \leq T \leq 1273$ K.

RESULTS AND DISCUSSION

XRD patterns of $Nd(Cr_{1-x}Co_x)O_3$ ($0 \leq x \leq 1.0$) were completely indexed as the orthorhombic perovskite-type ($GdFeO_3$-type) structure. Figure 1 shows the relationship between the cell constants (a, b, and c axes) and the composition. In the range $0 \leq x \leq 0.8$, the cell constants decrease linearly with increasing x. The observed cell constants of $NdCoO_3$ ($x = 1.0$) are larger by ≈0.0010 nm than the cell constants extrapolated from the values in the range $0 \leq x \leq 0.8$.

Figure 2 shows the relationship between the cell volume (V) of $Nd(Cr_{1-x}Co_x)O_3$ and the composition. The cell volume of $NdCrO_3$ ($x = 0$) is 0.2285 nm^3 and decreases linearly with increasing x. The observed cell volume of $NdCoO_3$ ($x = 1.0$) is 0.2151 nm^3 and is larger than the cell volume extrapolated from the values in the range $0 \leq x \leq 0.8$. The ionic radii of a Cr^{3+} ion, a Co^{3+} ion (low-spin state), and the Co^{3+} ion (high-spin state) with a coordination number (CN) of 6 are 0.0615, 0.0525, and 0.061 nm, respectively (9). The decrease in the cell volume is explained by the difference in the ionic radius between the Cr^{3+} and

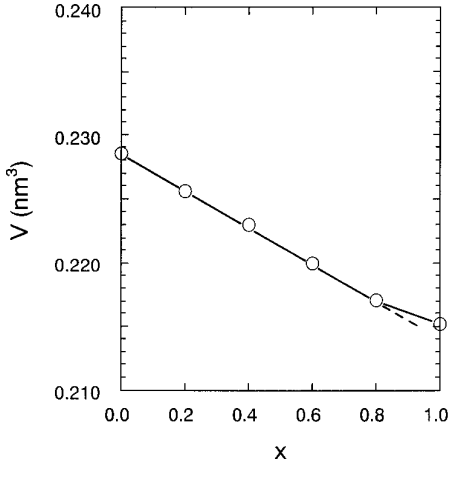

FIG. 2. Cell volume vs composition for the system $Nd(Cr_{1-x}Co_x)O_3$.

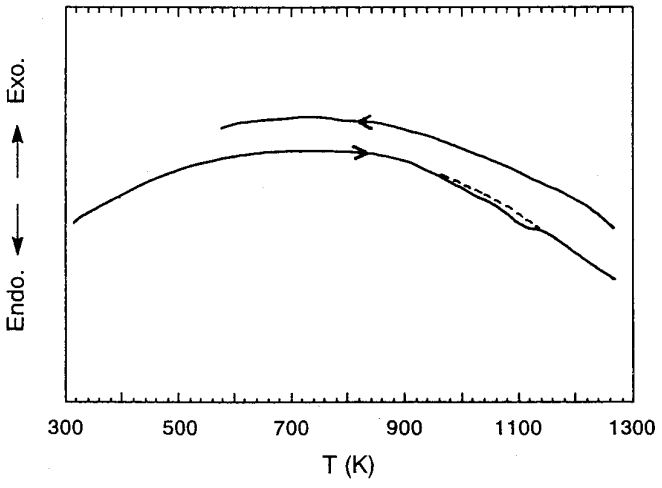

FIG. 3. DTA curve of $NdCoO_3$ ($x = 1.0$).

Co^{3+} ions, and the Co^{3+} ions must be in the low-spin state $(d\varepsilon)^6$ $(d\gamma)^0$.

Figure 3 shows DTA of $NdCoO_3$ ($x = 1.0$) in the interval $300 \leq T \leq 1273$ K. On heating, $NdCoO_3$ gave a broad and weak endothermic peak in the interval $920 \leq T \leq 1120$ K. However, $NdCoO_3$ gave no exothermic or endothermic peaks on cooling. The phase of the sample after the DTA measurement was identified by XRD. The diffraction pattern had both the peaks of orthorhombic perovskite-type $NdCoO_3$ and extra peaks. The extra peaks were very weak and were indexed as Nd_2O_3. From the results, it is considered that a little $NdCoO_3$ decomposed into Nd_2O_3 and cobalt oxides in the interval $920 \leq T \leq 1120$ K.

The structure refinement of $Nd(Cr_{1-x}Co_x)O_3$ ($0 \leq x \leq 1.0$) was carried out by Rietveld analysis of XRD data. $Nd(Cr_{1-x}Mn_x)O_3$ has the orthorhombic $GdFeO_3$-type structure with space group *Pnma* (8). Therefore, in the present study, it can be concluded that $Nd(Cr_{1-x}Co_x)O_3$ has the same structure with space group *Pnma* (11). Isotropic thermal parameters (B) for Nd, Cr, Co, O(1), and O(2) ions were refined assuming that they had the same values. Refined structural parameters and residuals, R_{WP}, R_I, and R_F are listed in Table 1. R_{WP}, R_I, and R_F are the weighted pattern, the integrated intensity, and the structure factor, respectively. The final R_F of all samples was less than 2.30%, and the low R_F suggests that the structural model for $Nd(Cr_{1-x}Co_x)O_3$ is reasonable.

In the orthorhombic $GdFeO_3$-type structure, A-site cations (Nd ions) coordinate with twelve anions; four O(1) and eight O(2) ions. B-site cations (Cr and Co ions) coordinate with six anions; two O(1) and four O(2) ions. The average (Cr, Co)–O distance of $Nd(Cr_{1-x}Co_x)O_3$ was calculated from the refined structural parameters and is shown in Fig. 4. The average Cr–O distance of $NdCrO_3$ ($x = 0$) is $\approx 0.1977 \pm 0.0014$ nm. In the range $0 \leq x \leq 0.8$, the

TABLE 1
Refined Structure Parameters for $Nd(Cr_{1-x}Co_x)O_3$

$x = 0.0$ $a = 0.54798(1)$ nm $b = 0.76918(2)$ nm $c = 0.54221(1)$ nm
$R_{WP} = 12.69\%$ $R_I = 2.01\%$ $R_F = 1.26\%$

Atom	Position	x	y	z	B
Nd	4(c)	0.041(1)	0.25	−0.008(1)	0.0028(6)
Cr	4(b)	0	0	0.5	0.0028(6)
O(1)	4(c)	0.484(4)	0.25	0.082(6)	0.0028(6)
O(2)	8(d)	0.292(4)	0.041(3)	−0.289(4)	0.0028(6)

$x = 0.2$ $a = 0.54489(2)$ nm $b = 0.76608(3)$ nm $c = 0.54050(2)$ nm
$R_{WP} = 11.66\%$ $R_I = 1.98\%$ $R_F = 1.28\%$

Atom	Position	x	y	z	B
Nd	4(c)	0.040(4)	0.25	−0.008(1)	0.0023(5)
Cr, Co	4(b)	0	0	0.5	0.0023(5)
O(1)	4(c)	0.491(4)	0.25	0.076(6)	0.0023(5)
O(2)	8(d)	0.288(4)	0.036(3)	−0.293(4)	0.0023(5)

$x = 0.4$ $a = 0.54208(2)$ nm $b = 0.76324(3)$ nm $c = 0.53901(2)$ nm
$R_{WP} = 11.28\%$ $R_I = 1.51\%$ $R_F = 1.21\%$

Atom	Position	x	y	z	B
Nd	4(c)	0.039(1)	0.25	−0.008(1)	0.0029(5)
Cr, Co	4(b)	0	0	0.5	0.0029(5)
O(1)	4(c)	0.491(4)	0.25	0.072(5)	0.0029(5)
O(2)	8(d)	0.283(5)	0.036(3)	−0.292(4)	0.0029(5)

$x = 0.6$ $a = 0.53873(4)$ nm $b = 0.75998(8)$ nm $c = 0.53718(5)$ nm
$R_{WP} = 16.47\%$ $R_I = 3.26\%$ $R_F = 1.99\%$

Atom	Position	x	y	z	B
Nd	4(c)	0.036(1)	0.25	−0.007(1)	0.0025(9)
Cr, Co	4(b)	0	0	0.5	0.0025(9)
O(1)	4(c)	0.490(7)	0.25	0.071(11)	0.0025(9)
O(2)	8(d)	0.284(10)	0.038(7)	−0.288(9)	0.0025(9)

$x = 0.8$ $a = 0.53532(2)$ nm $b = 0.75689(4)$ nm $c = 0.53565(3)$ nm
$R_{WP} = 17.04\%$ $R_I = 3.47\%$ $R_F = 2.30\%$

Atom	Position	x	y	z	B
Nd	4(c)	0.036(1)	0.25	−0.006(1)	0.0036(9)
Cr, Co	4(b)	0	0	0.5	0.0036(9)
O(1)	4(c)	0.495(8)	0.25	0.067(11)	0.0036(9)
O(2)	8(d)	0.281(11)	0.039(6)	−0.284(9)	0.0036(9)

$x = 1.0$ $a = 0.53312(1)$ nm $b = 0.75482(1)$ nm $c = 0.53461(1)$ nm
$R_{WP} = 14.01\%$ $R_I = 2.56\%$ $R_F = 2.20\%$

Atom	Position	x	y	z	B
Nd	4(c)	0.035(1)	0.25	−0.005(1)	0.0017(6)
Co	4(b)	0	0	0.5	0.0017(6)
O(1)	4(c)	0.495(5)	0.25	0.076(8)	0.0017(6)
O(2)	8(d)	0.287(6)	0.040(4)	−0.285(6)	0.0017(6)

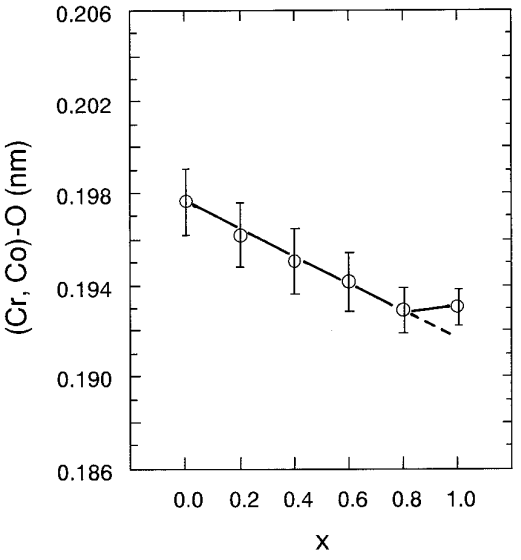

FIG. 4. Average (Cr, Co)–O distance vs composition for the system $Nd(Cr_{1-x}Co_x)O_3$.

average (Cr, Co)–O distance decreases linearly. The average Co–O distance of $NdCoO_3$ ($x = 1.0$) is $\approx$0.1931 $\pm$ 0.0008 nm, and this value is larger by $\approx$0.0014 nm than the average Co–O distance extrapolated from the values in the range $0 \leq x \leq 0.8$. Because the ionic radius of the Co^{3+} ion with the high-spin state is nearly equal to the ionic radius of the Cr^{3+} ion (9), the linear decrease of the average (Cr, Co)–O distance suggests that the Co^{3+} ion must be in the low-spin state $(d\varepsilon)^6(d\gamma)^0$. The angles for O–(Cr, Co)–O and (Cr, Co)–O–(Cr, Co) in $Nd(Cr_{1-x}Co_x)O_3$ are calculated from the refined structural parameters. The average angles for O(1)–(Cr, Co)–O(1), O(1)–(Cr, Co)–O(2), and O(2)–(Cr, Co)–O(2) are 180°, 90°, and 90° or 180°, respectively. From the results of the average (Cr, Co)–O distances and the average angles for O–(Cr, Co)–O, it is obvious that each $(Cr, Co)O_6$ octahedron has little distortion. The average angles for (Cr, Co)–O(1)–(Cr, Co) and (Cr, Co)–O(2)–(Cr, Co) are less than 180° and are shown in Fig. 5. In the range $0 \leq x \leq 0.8$, the average angles for both (Cr, Co)–O(1)–(Cr, Co) and (Cr, Co)–O(2)–(Cr, Co) increase linearly with increasing x. However, the average angles for both Co–O(1)–Co and Co–O(2)–Co in $NdCoO_3$ ($x = 1.0$) are $\approx$155.6° and 155.7°, respectively. These values are larger than the extrapolated values.

The temperature dependence of the inverse magnetic susceptibility ($1/\chi$) of $Nd(Cr_{1-x}Co_x)O_3$ ($0 \leq x \leq 1.0$) is shown in Fig. 6. $NdCrO_3$ ($x = 0$) and $Nd(Cr_{0.8}Co_{0.2})O_3$ ($x = 0.2$) are antiferromagnetic with $T_N \approx 220$ K and $T_N \approx 180$ K, respectively. However, $Nd(Cr_{1-x}Co_x)O_3$ ($0.4 \leq x \leq 1.0$) is paramagnetic above 80 K. The $1/\chi$-T curves obey the Curie–Weiss law below $\approx$630 K ($x = 0$), 490 K ($x = 0.2$), 450 K ($x = 0.4$), 380 K ($x = 0.6$), 270 K ($x = 0.8$), and 210 K ($x = 1.0$). These temperatures are defined as T_M, and are shown as the arrows in Fig. 6. The $1/\chi$-T curve of $Nd(Cr_{1-x}Co_x)O_3$ resembles that of $LaCoO_3$ (2). In $LaCoO_3$, both the low-spin and high-spin states of the Co^{3+} ions coexist in the interval $110 < T < 350$ K, and the $1/\chi$-T curve exhibits a plateau in the interval $450 < T < 650$ K. The plateau indicates a temperature interval where there is a conversion from one stable spin configuration at cobalt ions to another. Above 650 K, both the high-spin and intermediate-spin states of the Co^{3+} ions coexist.

The effective magnetic moment (μ_{eff}) was calculated from the region that obeyed the Curie–Weiss law. Figure 7 shows the relationship between μ_{eff} of $Nd(Cr_{1-x}Co_x)O_3$ and the composition. The theoretical μ_{eff} is calculated using

$$\mu_{eff} = \sqrt{(1-x)\mu^2_{Cr^{3+}} + x\mu^2_{Co^{3+}} + \mu^2_{Nd^{3+}}},$$

where $\mu_{Cr^{3+}}$, $\mu_{Co^{3+}}$, and $\mu_{Nd^{3+}}$ are the effective magnetic moment of the Cr^{3+} ion, the Co^{3+} ion, and the Nd^{3+} ion, respectively (12). From the values of the spectroscopic splitting factor (g) and the total angular momentum (J) of the Nd^{3+} ion, $\mu_{Nd^{3+}}$ is calculated to be 3.62 (8). In Fig. 7, the broken lines (1) and (2) indicate the theoretical values calculated in cases of both the high-spin and the low-spin states of the Co^{3+} ion; the line (1) is the high-spin state $(d\varepsilon)^4(d\gamma)^2$ and the line (2) is the low-spin state $(d\varepsilon)^6(d\gamma)^0$. From the results of Fig. 7, it is obvious that the spin state of the Co^{3+} ion in $Nd(Cr_{1-x}Co_x)O_3$ is low below T_M. Above T_M, the $1/\chi$-T curve exhibits the plateau, and this plateau must be the conversion from the low-spin state of the Co^{3+} ion to the mixed spin state.

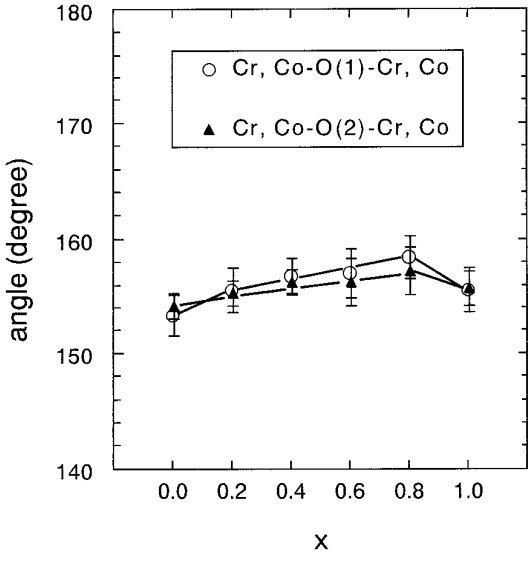

FIG. 5. Angles for (Cr, Co)–O(1)–(Cr, Co) and (Cr, Co)–O(2)–(Cr, Co) vs composition for the system $Nd(Cr_{1-x}Co_x)O_3$.

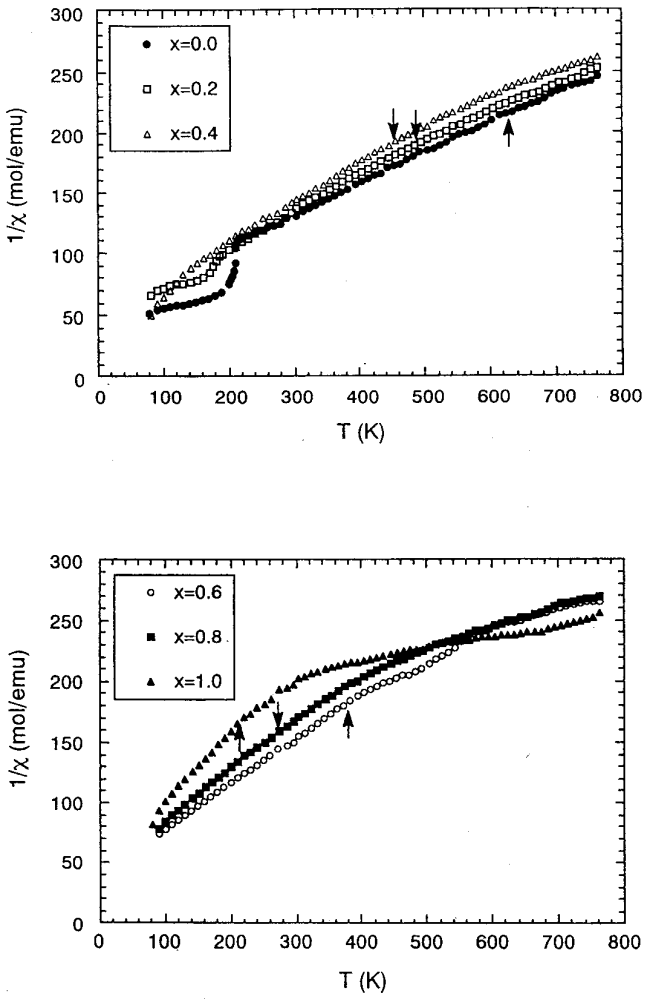

FIG. 6. Inverse magnetic susceptibility ($1/\chi$) vs temperature (T) for the system $Nd(Cr_{1-x}Co_x)O_3$.

The relationship between the logarithm of the electrical resistivity (log ρ) of $Nd(Cr_{1-x}Co_x)O_3$ and the reciprocal temperature ($1000/T$) is shown in Fig. 8. The decrease of log ρ with increasing temperature indicates that $Nd(Cr_{1-x}Co_x)O_3$ is a semiconductor. The log ρ-$1000/T$ curves are linear below ≈560 K ($x = 0$), 460 K ($x = 0.2$), 420 K ($x = 0.4$), 370 K ($x = 0.6$), 330 K ($x = 0.8$), and 240 K ($x = 1.0$). These temperatures are defined as T_R, and are shown as the arrows in Fig. 8. The energy gaps (E_g) calculated from the linear portion of log ρ-$1000/T$ curves are ≈0.45 eV ($x = 0$), 0.47 eV ($x = 0.2$), 0.38 eV ($x = 0.4$), 0.38 eV ($x = 0.6$), 0.36 eV ($x = 0.8$), and 0.37 eV ($x = 1.0$).

T_M is nearly equal to T_R; that is, the region that obeyed the Curie–Weiss law agrees with the linear portion of the log ρ-$1000/T$ curves. The spin state of the Co^{3+} ion is low below T_M, and the low-spin state of the Co^{3+} ion converts to another above T_M. T_M for $NdCoO_3$ ($x = 1.0$) is below room temperature, and the spin state of the Co^{3+} ion varies partly from low to another. In the present study, XRD data were collected at room temperature. Therefore, both the average Co–O distance and the average angles for Co–O(1 and 2)–Co are larger than the extrapolated values, and the log ρ-$1000/T$ curves are strongly affected by the spin state of the Co^{3+} ion.

The (Cr, Co)O_6 octahedron in $Nd(Cr_{1-x}Co_x)O_3$ connects with O(1) or O(2) of the other (Cr, Co)O_6 octahedron. The Cr^{3+} ion has the electron configuration $(d\varepsilon)^3(d\gamma)^0$, and the Co^{3+} ion has the electron configuration $(d\varepsilon)^6(d\gamma)^0$ or $(d\varepsilon)^4(d\gamma)^2$. There are two kinds of the cation–anion–cation overlap; one is an overlap (π bonding) between the cation $d\varepsilon$ and oxygen p_π orbitals, and the other is the overlap (σ bonding) between the cation $d\gamma$ and oxygen p_σ orbitals. According to Goodenough (13), three $3d$ electrons of the Cr^{3+} ion in $LaCrO_3$ are all localized and the Fermi level lies between the filled $d\varepsilon^*$ levels and the narrow $d\gamma^*$ levels. Rao *et al.* (14) proposed that the Cr^{4+} ions present as a result of impurities or native defects give rise to p-type extrinsic conduction in $LaCrO_3$. Below T_M (or T_R), $Nd(Cr_{1-x}Co_x)O_3$ is the semiconductor with E_g of ≈0.36–0.47 eV, and the $d\varepsilon^*$ level is filled by $3d$ electrons and the $d\gamma^*$ level is empty. Both the $d\varepsilon^*$ and $d\gamma^*$ levels are localized and narrow, and the cation–anion–cation overlap integrals (Δ^π_{cac} for π bonding and Δ^σ_{cac} for σ bonding) are smaller than the critical overlap integral (Δ_C); $\Delta^\pi_{cac} < \Delta^\sigma_{cac} < \Delta_C$ (15). The intra-atomic exchange (Δ_{ex}) between the $d\varepsilon^*$-α and $d\varepsilon^*$-β levels is larger than the crystal-field splitting (10Dq) between the $d\varepsilon^*$ and $d\gamma^*$ levels. If the

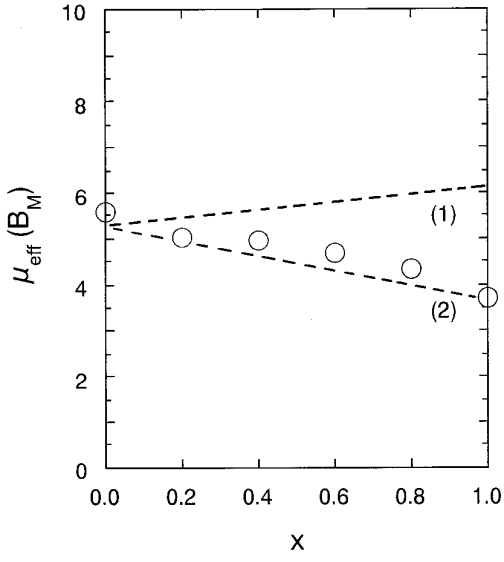

FIG. 7. Effective magnetic moment (μ_{eff}) vs composition for the system $Nd(Cr_{1-x}Co_x)O_3$. The broken lines (1) and (2) indicate the theoretical values calculated in cases of both the high-spin and low-spin states of the Co^{3+} ion; the line (1) is the high-spin state $(d\varepsilon)^4(d\gamma)^2$ and the line (2) is the low-spin state $(d\varepsilon)^6(d\gamma)^0$.

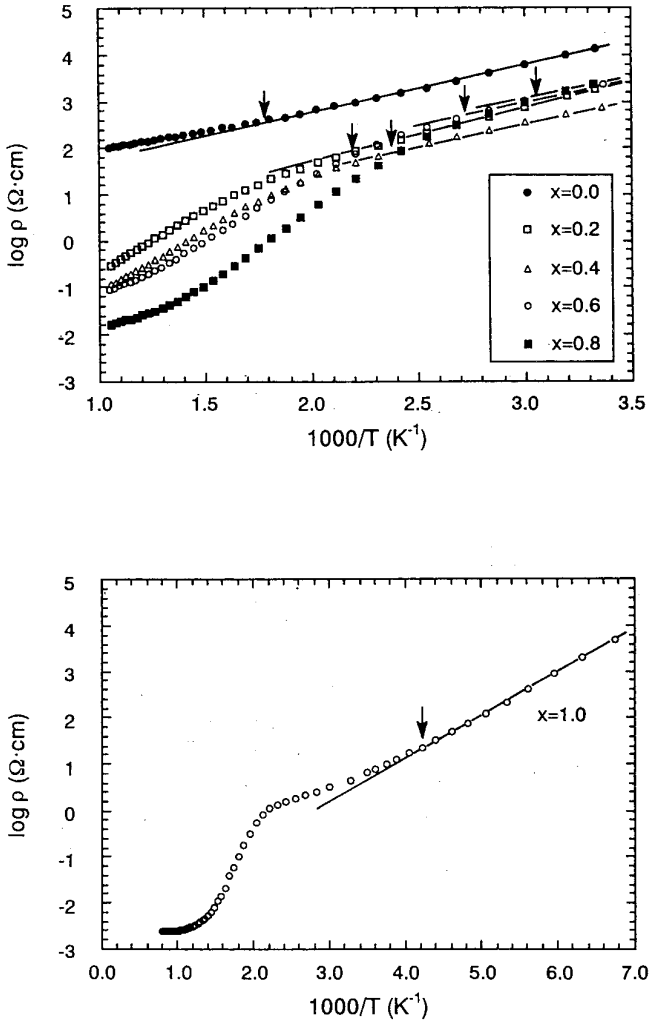

FIG. 8. Logarithm of the electrical resistivity (log ρ) vs $1000/T$ for the system $Nd(Cr_{1-x}Co_x)O_3$.

average (Cr, Co)–O distance is independent of the composition, it is obvious that the overlap between the cation $d\varepsilon$ and oxygen p_π orbitals increases with the average angle for (Cr, Co)–O(1 and 2)–(Cr, Co) approaching 180°, and π bonding becomes strong (8). Both the linear decrease of the average (Cr, Co)–O distance and the linear increase of the number of $3d$ electrons with increasing x make π bonding increase, and make 10Dq decrease. Therefore, the decrease of log ρ and E_g with increasing x was observed. Above T_M (or T_R), the spin state of the Co^{3+} ion changes from low to another, the average angles for (Cr, Co)–O(1 and 2)–(Cr, Co) deviate from 180°, and the $d\gamma^*$ level is partly filled by $3d$ electrons. Although π bonding becomes weak with increasing temperature, the transfer of the electrons through σ bonding becomes active. From these results, it is apparent that the cation–anion–cation overlap is strongly affected by the spin state of the Co^{3+} ion.

CONCLUSION

I have shown that the magnetic and electrical properties of $Nd(Cr_{1-x}Co_x)O_3$ depend on the spin state of the Co^{3+} ion and the cation–anion–cation overlap. The decrease of the average (Cr, Co)–O distance and μ_{eff} indicate that the Co^{3+} ion in $Nd(Cr_{1-x}Co_x)O_3$ is in the low-spin state $(d\varepsilon)^6(d\gamma)^0$ below T_M. Above T_M, the $1/\chi$-T curve exhibits the plateau, and this plateau exhibits the conversion from the low-spin state of the Co^{3+} ion to the mixed spin state. Below T_M (or T_R), the log ρ-$1000/T$ curves indicate that $Nd(Cr_{1-x}Co_x)O_3$ is semiconductive with E_g of $\approx$0.36–0.47 eV. The log ρ-$1000/T$ curves above T_M (or T_R) deviate from that below T_M (or T_R).

ACKNOWLEDGMENTS

The author expresses his thanks to Dr. H. Kido, Osaka Municipal Technical Institute for the magnetic measurements. The present work was supported by Grant-in-Aid for Science Research 06453078 from the Ministry of Education, Science, and Culture of Japan.

REFERENCES

1. P. M. Raccah and J. B. Goodenough, *Phys. Rev.* **155,** 932 (1967).
2. M. A. Senaris-Rodriguez and J. B. Goodenough, *J. Solid State Chem.* **116,** 224 (1995).
3. W. H. Madhusudan, K. Jagannathan, P. Ganguly, and C. N. R. Rao, *J. Chem. Soc. Dalton Trans.* 1397 (1980).
4. G. Demazeau, M. Pouchard, and P. Hagenmuller, *J. Solid State Chem.* **9,** 202 (1974).
5. T. Arakawa, S. Tsuchi-Ya, and J. Shiokawa, *Mater. Res. Bull.* **16,** 97 (1981).
6. J. B. Goodenough and J. M. Longo, *in* "Landolt-Bornstein, Numerical Data and Functional Relationships in Science and Technology. New Series, Group 3, Vol. 4, Magnetic and Other Properties of Oxides and Related Compounds" (K. H. Hellwege, Ed.), p. 228. Springer-Verlag, New York, 1971.
7. H. Taguchi, M. Nagao, and Y. Takeda, *J. Solid State Chem.* **114,** 236 (1995).
8. H. Taguchi, *J. Solid State Chem.* **118,** 367 (1995).
9. R. D. Shannon and C. T. Prewitt, *Acta Crystallogr. Sect. B* **25,** 925 (1969).
10. F. Izumi, *Nippon Kesho Gakkaishi* **27,** 23 (1985). [Japanese]
11. K. R. Poeppelmeier, M. E. Leonowicz, J. C. Scanlon, and W. B. Yelon, *J. Solid State Chem.* **45,** 71 (1982).
12. T. Shin-Ike, T. Sakai, G. Adachi, and J. Shiokawa, *Mater. Res. Bull.* **12,** 831 (1977).
13. J. B. Goodenough, *J. Appl. Phys.* **37,** 1415 (1966).
14. G. V. Rao, B. M. Wanklyn, and C. N. R. Rao, *J. Phys. Chem. Solids* **32,** 345 (1971).
15. J. B. Goodenough, *Czech. J. Phys. B* **17,** 304 (1967).